CONFERENCE PRE-PRINT

# LEVERAGING TURBULENCE DATA FROM FUSION EXPERIMENTS

M.J. CHOI, J.-M. KWON, J.W. KIM
Korea Institute of Fusion Energy
Daejeon, Republic of Korea
Email: mjchoi@kfe.re.kr

G.J. CHOI
Korea Advanced Institute of Science & Technology
Daejeon, Republic of Korea

T.S. Hahm
Seoul National University
Seoul, Republic of Korea

**Abstract**

Recent advance in plasma diagnostics allows turbulent fluctuation measurements of plasma density or temperature even in two-dimensional space in fusion experiments. Extracting more information from turbulence data would be crucial for a deeper understanding of plasma turbulence transport. In this manuscript, some spectral and statistical analysis methods that can be complementary to each other are introduced along with their application revealing distinguished pedestal turbulence characteristics between the spontaneous edge localized mode (ELM) free phase and the ELM suppression phase by the resonant magnetic perturbation (RMP) field. In the former case, the saturation mechanism of the pedestal turbulence can be identified. The turbulence was saturated by modulational couplings between high frequency pump modes and low frequency modulating modes, and the fluctuations exhibit a chaotic behavior. In the latter case, the growth mechanism of the pedestal turbulence can be discussed with observations that are not inconsistent with relevant theories and numerical simulations. The strong bicoherence and chaotic behavior in low frequency fluctuations implies that the resonance between a magnetic island and drift waves might be responsible for the enhancement of low-k fluctuations during the RMP ELM suppression transition. On the other hand, the stochastic behavior in high frequency (high-k) fluctuations suggests that these fluctuations might arise in associated with tangled small scale magnetic fields around the island. Besides these conventional analyses, further methods for leveraging the turbulence data with the physics informed neural network would be also discussed.

## 1. INTRODUCTION

Fluctuation measurements of various plasma fields such as density and electron temperature are now routinely available in many fusion plasma experiments [1]. The beam emission spectroscopy (BES) and the microwave imaging reflectometry (MIR) have been developed to measure the local plasma density fluctuation, and the electron cyclotron emission imaging (ECEI) diagnostics for the electron temperature fluctuation. Their analyses have revealed various characteristics of low-k plasma turbulence and advanced our understanding of turbulence transport in fusion experiments.

In this paper, analysis methods for leveraging the measured turbulent fluctuation data [2] are briefly introduced with some examples. Depending on purposes and conditions, a proper analysis method or the combination of methods can be used to extract more information from data. The linear and nonlinear spectral methods can provide the frequency or wavenumber spectrum and detect high order couplings among fluctuation components (Section 2). These methods would be effective when there exist a few dominant coupling processes per each coupled triad (or quartet). To deal with more complicated systems with the large number of nonlinear couplings, the statistical perspective and methods would be helpful (Section 3). The spectral and statistical methods can be complementary to reveal in-depth information buried in fluctuation data. As an example, the distinguished characteristic of pedestal electron temperature fluctuations between the spontaneous edge localized mode (ELM) free phase and the ELM suppression phase by the resonant magnetic perturbation (RMP) field would be demonstrated (Section 4). In addition, it would be discussed that recent developments of the physics informed neural network can allow leveraging turbulence data in novel ways including the turbulence model validation and the prediction of a missing field (Section 5).

## 2. SPECTRAL METHODS

### 2.1 Frequency spectrum

A frequency spectrum is the most fundamental analysis of time series data, providing an estimate of fluctuation power at each frequency. The discrete Fourier transform (DFT) is often used to estimate the frequency spectrum of uniformly discrete stationary time series data [3]. The wavelet [4] or the maximum entropy method [5] based spectrum can be also considered when a stationary analysis period is too short or the obtained data length is limited. Or, if the data is sampled unevenly, the Lomb-Scargle periodogram [6] can be used to estimate the frequency spectrum.

There is always noisy component in the measured signal from real experiments, and identifying or suppressing noise levels in the frequency spectrum has been of particular importance. One of well-known methods to suppress noises utilizes that noises are often rapidly decorrelated in time or space [7]. Thermal noise and shot noise are typical examples of noises characterized by short correlation ranges. Diagnostic channels can be prepared to be separated by a proper distance that is sufficient for noises to be decorrelated but still within the correlation range of a physical component. For example, decorrelated noises in two time series data $x$ and $y$, obtained by channels separated by a spatial distance $\boldsymbol{d}$, can be reduced by the ensemble average in calculation of the cross-power spectrum $\langle XY^* \rangle$, while the physical component remains because of its coherent phase relationship $\delta_{xy} = \boldsymbol{k} \cdot \boldsymbol{d}$ which is characterized by the wavenumber $\boldsymbol{k}$ of the physical component (see Fig. 1).

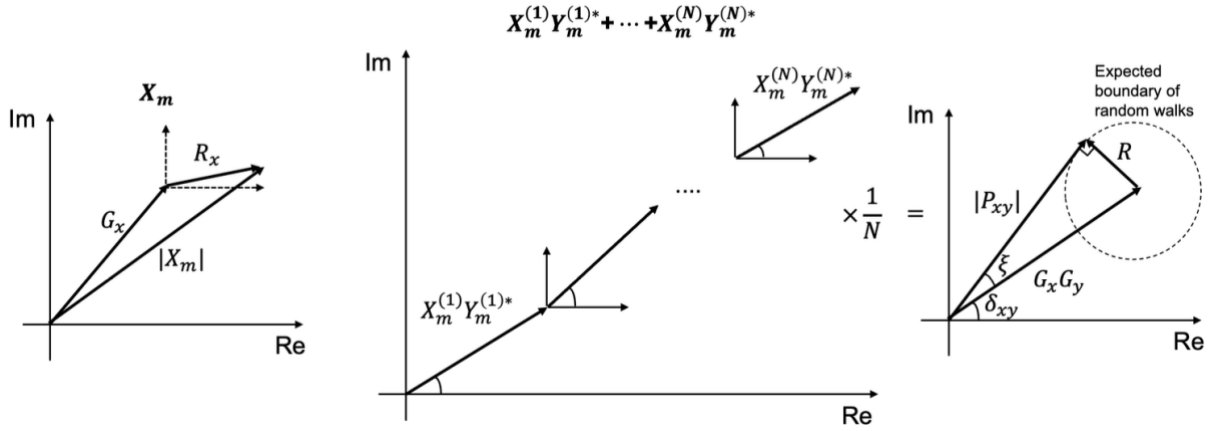


*FIG. 1. The Fourier transform coefficient ($X$ or $Y$) contains both a physical component ($G_x$ or $G_y$) and an additive noise component ($R_x$ or $R_y$). The auto-power spectrum $\langle XX^* \rangle$ provides the estimate of the total power. The cross-power spectrum $\langle XY^* \rangle$ with the large number of ensemble ($N$) can suppress the noise component, i.e., $P_{xy} \approx G_xG_y$, because adding up the components with the random phase would be like the random walk in the complex plane, whose the amplitude ($R$) and phase deviation ($\xi$) decay with $N$.*

The above noise suppression method, however, cannot be applicable if either the noise is not additive and has a long correlation time or the multi-measurements are not available. Firstly, we can consider a situation where a multiplicative component with the long correlation time is involved, instead of an additive and short-correlated noise. Signals of fusion plasma turbulence diagnostics can depend on the product of multiple plasma fields such as density and temperature, and if one of them exhibits a long correlated noisy character, then it can distort the ordinary DFT based spectral analysis and hinder the identification of a Fourier mode in the other field. In such a case, the Laplace or robust coherence [8] can be used to identify the Fourier mode. It utilizes the median regression to find the Fourier coefficients, making it more robust against the outliers. Secondly, when we have only a single measurement, the orthogonal wavelet based denoising method can be considered [9]. Based on a priori assumption that the noise is additive and white-Gaussian, and a recursive algorithm was devised to estimate a noise level in each step during which the wavelet coefficients smaller than the noise level are removed. The noise characteristic can be checked a posteriori.

### 2.2 Nonlinear mode coupling

The higher order spectral methods can be used to detect the mode-mode coupling in signals. These methods are based on a definite phase relation among the coupled Fourier modes. For example, a nonlinear three-wave

coupling can be identified using bicoherence [10], and a four-wave coupling using tricoherence [11]. For the two-dimensional representation of a modulational four-wave coupling, a modulogram was devised as follows [12].

$$\mathrm{MG}(f_p, f_m) = \langle X^2(f_p) X^*(f_p + f_m) X^*(f_p - f_m) \rangle$$

It can detect the spectral coupling among a pump wave $f_p$, an amplitude modulating wave $f_m$, and two sidebands $f_p \pm f_m$.

## 3. STATISTICAL METHODS

Spectral methods to detect nonlinear couplings introduced in the previous section would be effective when there exist only a few dominant coupling processes per each triad (or quartet), keeping the (temporarily) coherent phase relationships identifiable. In a more complicated system composed of the great number of comparable and interchanging nonlinear couplings, it may be difficult to expect one particular nonlinear relationship to be distinguished from others. Then, the evolution of a physical quantity $\phi(t)$ can be described using a Langevin-type equation where effects of all processes are summed up into a stochastic process: $\phi(t) = \phi_0 + \int_0^t dt'\, \xi(t')$.

### 3.1. Gaussian or non-Gaussian

One may think that the most natural choice for the distribution of $\xi(t)$ is a Gaussian distribution, stemming from the central limit theorem (CLT). The CLT states that a sum of $N$ independent and identically distributed random variables, $s_N = \sum_{n=1}^{N} x_n$, obeys a Gaussian distribution as $N \to \infty$ when the first and second moments of $x_n$ do not diverge. It is actually a special case of the limiting ($N \to \infty$) distribution for the sum $s_N$ when $x_n$ has the finite moments. Mathematically, any stable distribution can be the limiting distribution of $s_N$ for some $x_n$, and the Gaussian distribution is a special case of Lévy stable distributions. When the distribution of $x_n$ itself has a power-law heavy tail not to have finite first or second moment, the limiting distribution of $s_N$ becomes a non-Gaussian Lévy distribution. The Gaussian distribution is not the only natural choice for the distribution of $\xi(t)$.

Analysis of statistical properties of measured turbulence data would provide a hint on the underlying process. Calculating the higher order moments (skewness or kurtosis) of the $\phi(t)$ increments, $\Delta\phi(\tau) = \phi(t+\tau) - \phi(t)$, can tell whether the underlying distribution is close to a Gaussian or not. Skewness (Kurtosis) close to zero (three) corresponds to a Gaussian distribution, and they deviate from those values for a non-Gaussian distribution. Non-zero skewness (non-three kurtosis) implies that the finite bicoherence (tricoherence) is identifiable.

### 3.2 Stochastic or chaotic

Whether measured turbulence data is close to signals generated by a stochastic process such as the fractional Brownian motion (fBm) and the fractional Gaussian noise (fGn) or chaotic signals generated from deterministic systems having a low dimensional nonlinearity can be distinguished using the complexity-entropy analysis [13]. Here, entropy and complexity are information theoretic terminologies with specific meanings. Entropy means a measure of missing (unknown) information of the given probability distribution. It has the maximum for the equiprobable distribution because one can learn almost nothing from the equiprobable distribution. Complexity was suggested as the product of disequilibrium and entropy (missing information) to capture the intuitive notion about a complex system [14]. Disequilibrium is a measure of distance from the equiprobable distribution. The Jensen Shannon divergence is used for disequilibrium for the complexity-entropy analysis [13]. The idea of complexity can be understood by two examples [14] of simple (not complex) system in physics, i.e., a perfect crystal and an ideal gas. A perfect crystal, represented by a peaked probability distribution of states, has very small missing information but large disequilibrium, and their product complexity will remain small. On the other hand, an ideal gas, represented by an equiprobable distribution of states, has large missing information but very small disequilibrium, and their product complexity also will remain small. It was shown that signals from various chaotic systems (the logistic map, the skew tent map, Henon's map, etc.) and signals from stochastic processes (fBm and fGn) can be separated in the complexity-entropy plane [13].

The analysis starts with calculating the probability distribution of amplitude orders in partial segments of given time series data, called the Bandt-Pompe (BP) probability distribution [15]. Using the BP probability distribution of a given data $P = \{p_j\}_{j=1,\ldots,d!}$ where subscript $i$ represents each amplitude order, the Jensen Shannon complexity $C_{\mathrm{JS}}$ and the normalized Shannon entropy $H$, which are the basis of the complexity-entropy analysis,

can be calculated. The Jensen Shannon complexity ($C_{\mathrm{JS}} = QH$) is defined as the product of the normalized Shannon entropy $H = \frac{S}{S_{\max}}$ and the Jensen Shannon divergence $Q$. Here, $S = S(P) = -\sum_j p_j \ln(p_j)$ is the Shannon entropy of the given BP probability distribution and $S_{\max}$ is the maximum possible Entropy, i.e., $S_{\max} = \ln(d!)$ with the equiprobable distribution $P_{\mathrm{e}} = \{p_j\} = \frac{1}{d!}$. The Jensen Shannon divergence is given as $Q = Q_0 \left\{ S\left(\frac{P+P_e}{2}\right) - S\left(\frac{P}{2}\right) - S\left(\frac{P_e}{2}\right) \right\}$ where $Q_0$ is the normalization constant $Q_0 = -2/(\frac{d!+1}{d!}\ln(d!+1) - 2\ln(2d!) + \ln(d!))$. Chaotic signals locate close to the maximum complexity boundary in the complexity-entropy plane, and they move to the locus of points of fBm and fGn signals in proportion to the level of the additive Gaussian noise [16].

The rescaled complexity was suggested as a simple evaluation metric for the degree of chaos in signals [17]. It is defined as follows.

$$\hat{C} = \frac{C_{\mathrm{JS}} - C_0}{|C_{\mathrm{bdry}} - C_0|}$$

where $C_0$ is the Jensen Shannon complexity of fBm or fGn and $C_{\mathrm{bdry}}$ is the maximum (if $C_{\mathrm{JS}} > C_0$) or minimum (if $C_{\mathrm{JS}} < C_0$) Jensen Shannon complexity at the given $H$. The rescaled complexity ($\hat{C}$) ranges from -1 ($C_{\mathrm{JS}} = C_{\min}$) to 1 ($C_{\mathrm{JS}} = C_{\max}$), and the less $\hat{C}$ means the less chaotic or the more stochastic in the relative comparison.

## 4. DISTINGUISHED CHARACTERISTICS OF PEDESTAL TURBULENCE

### 4.1. Spontaneous ELM-free phase

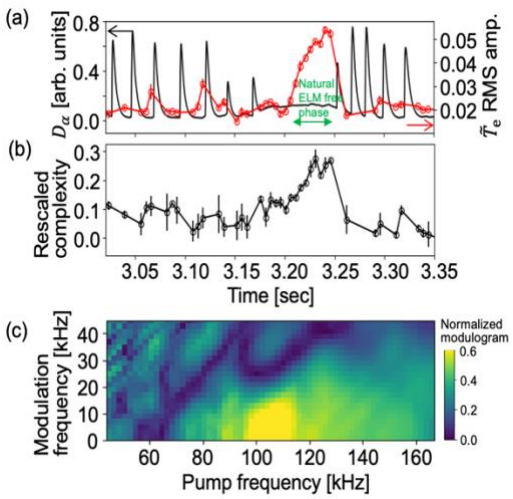


*FIG. 2. (a) The $D_\alpha$ emission (black) and the root mean square (RMS) amplitude of the normalized $T_e$ fluctuation at the pedestal top. (b) The rescaled complexity of the $T_e$ fluctuation. (c) Modulogram for a fluctuation saturation period.*

In the KSTAR H-mode plasmas, the growth and saturation of the broadband (0—170 kHz) electron temperature ($T_{\mathrm{e}}$) fluctuation near the pedestal top are observed for a short spontaneous ELM-free phase (Fig. 2(a)) [17]. The appearance of ELM-free phase seems to be related with the enhanced particle flux (the $D_\alpha$ baseline was noticeably increased during the ELM-free phase). The enhanced $T_{\mathrm{e}}$ fluctuation might contribute to the enhanced particle flux, but this is uncertain (the fluctuation level jumps significantly after 3.20 sec, but not the $D_\alpha$ baseline) and not discussed here. Instead, the fluctuation characteristics and the saturation process of turbulent fluctuation are investigated.

The zonal flow generation via the modulational instability of drift waves is one possible route of the nonlinear saturation of drift wave turbulences [18, 19]. A linearly unstable pump mode is saturated by the nonlinear energy transfer to the sidebands and the zonal flow. According to this scenario, the nonlinear oscillations between the zonal flows and the drift wave intensity can exhibit a chaotic behavior at the certain parameter regime [19].

Complementary analyses using both spectral and statistical methods suggest that turbulent $T_{\mathrm{e}}$ fluctuations in the KSTAR ELM-free pedestal are saturated via the modulational instability and the modulational coupling among the fluctuations results in the more chaotic behavior of the fluctuation, which is not inconsistent with the theoretical scenario [19]. Modulogram of the $T_{\mathrm{e}}$ fluctuation in Fig. 2(c) reveals four-wave couplings among pump modes (~100 kHz), low frequency modulating modes (< 20 kHz), and the sidebands when the total integrated RMS amplitude of the fluctuation is saturated. Also, the rescaled complexity of the $T_{\mathrm{e}}$ fluctuation in Fig. 2(b) shows that the fluctuation becomes more chaotic during the saturation phase. This example demonstrates that complementary spectral and statistical methods allow for extracting more comprehensive information about turbulence saturation process.

### 4.2. RMP ELM suppression phase

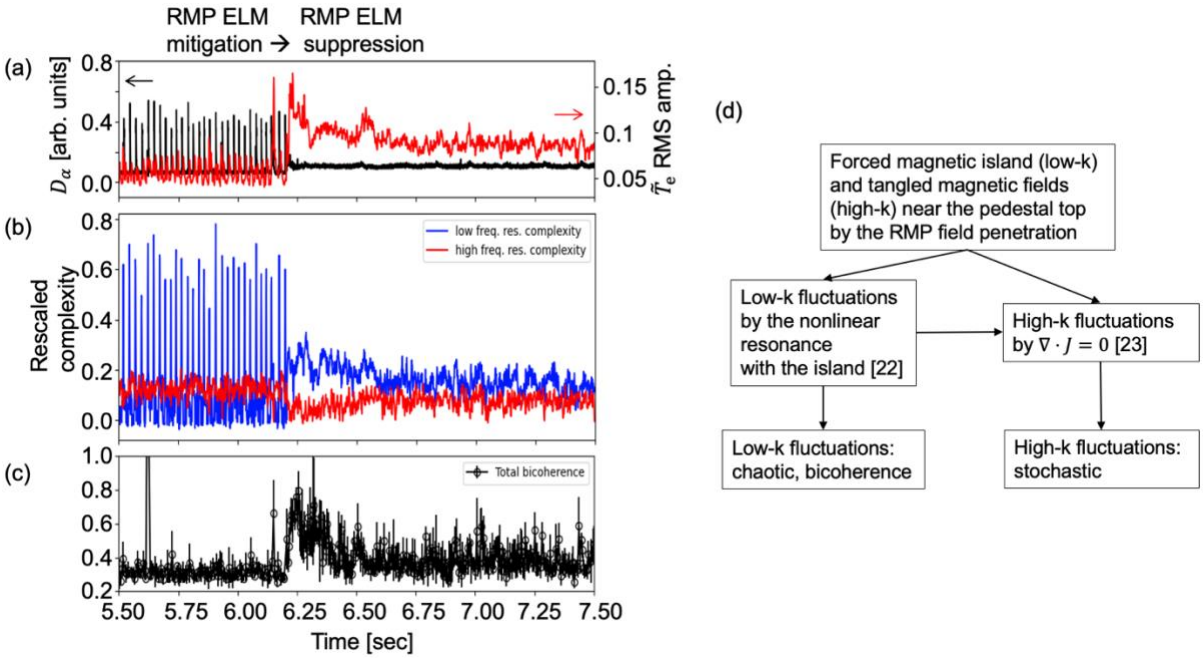


*FIG. 3. (a) The $D_\alpha$ emission (black) and the root mean square (RMS) amplitude of the normalized $T_e$ fluctuation at the pedestal top. (b) The rescaled complexity of the low (< 20 kHz) and high (> 20 kHz) frequency components of $T_e$ fluctuation. (c) Total bicoherence in the low frequency components of $T_e$ fluctuation. (d) A physical interpretation of observations.*

In the KSTAR $n = 1$ RMP ELM suppression experiment [20], the transition from the RMP ELM mitigation to the RMP ELM suppression is accompanied by the significant growth of broadband (0—70 kHz) $T_e$ fluctuations as shown in Fig. 3(a). Note that these fluctuations exhibit an almost linear dispersion relation in the laboratory frame. The nonlinear coupling and the statistical characteristics of the fluctuation is investigated to understand the origin of the fluctuations, which is summarized in Fig. 3(d).

The bicoherence analysis finds that the strength of three-wave couplings among fluctuations below 20 kHz is increased in correlation with the growth of the fluctuation during the ELM suppression transition as shown in Fig. 3(c). It is peaked at the early phase of the ELM suppression and maintained at the higher level (than that in the ELM mitigation phase) for the entire ELM suppression phase.

A numerical study suggests that the RMP field penetration and the onset of a magnetic island near the pedestal top can lead to the ELM suppression [21]. Also, a theoretical study shows that drift waves can arise from the resonance with a magnetic island of the comparable size when the island frequency is in between the electric drift frequency and the diamagnetic drift frequency [22]. The frequency condition can be satisfied at the moment of the RMP field penetration [17]. The enhanced low-k (low-frequency) fluctuations and bicoherence among them can be attributed to the nonlinear resonance between the island and drift waves.

On the other hand, the rescaled complexity analysis reveals that the enhanced high-k (high-frequency) fluctuations after the ELM suppression exhibit a relatively stochastic behavior, while the low-k fluctuations are more chaotic as expected from their enhanced bicoherence. Given the low-k fluctuations and high-k magnetic field perturbations, a theoretical study shows that the high-k fluctuations can arise to maintain the quasi-neutrality condition at all scales [23]. These high-k fluctuations, coupled to the tangled high-k fields around the island, can exhibit the stochastic behavior as indicated by the lowered rescaled complexity.

## 5. APPLICATION OF PHYSICS INFORMED NEURAL NETWORKS

The above example of turbulence data analysis shows that complementary spectral and statistical methods can allow a deeper understanding of the fluctuation characteristics. However, these analyses should have been extended if fluctuation measurements of additional plasma fields such as the velocity field were available.

Compared to measurements of plasma density and electron temperature fluctuations, accurate and high-resolution measurement of velocity fluctuation is more challenging in fusion plasmas. Direct measurement of the velocity

fluctuation is often limited in the particular wavenumber or real space. Indirect methods utilizing two-dimensional density or temperature fluctuation measurements in time are vulnerable to noises [24].

Recently, the missing field prediction using the physics informed neural network (PINN) [25—27] and measurements of other physically related fields has been demonstrated [28]. For the practical application for two-dimensional turbulent velocity field prediction in fusion plasmas, effects of the noise and the spatial resolution of available data are investigated in the two-dimensional Navier-Stokes system and the Hasegawa-Wakatani (HW) system, respectively [2]. These investigations show that missing fields of a physical system can be predicted better when the signal-to-noise ratio and the spatial resolution of the provided data are higher. As an example, Fig. 4 shows that the PINN can learn a solution of HW equations that matches the density ($n$) data, predicting the missing potential ($\phi$) and vorticity ($\Omega$) fields. The density data were taken at regular spatial and temporal intervals as in the experiment, and provided to train PINN with additional constraints from HW equations. As the spatial resolution of provided density data is varied, the PINN could capture the key characteristics of the potential field down to the 12 x 6 resolution case.

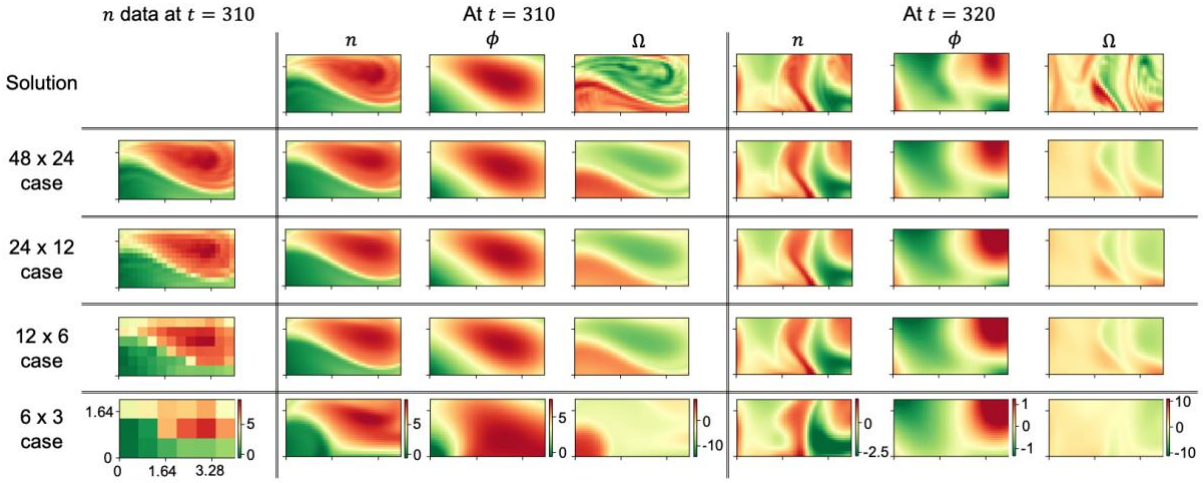


*FIG. 4. The PINN predictions of the density, potential, and vorticity fields in the Hasegawa-Wakatani system as the spatial resolution of provided density data is varied. Only the density measurements were provided to train the PINN with additional constraints from physics laws. The solution is shown at the top for reference.*

However, the missing field prediction using PINNs relies on the validity of the physics model, which leads to the problem of a turbulence model validation. The conventional wisdom in turbulence model validation is that only (ensemble averaged or time averaged) statistics of a model can be tested, not its dynamics. This is because turbulence model equations often include nonlinear terms exhibiting a chaotic behavior and matching initial and boundary conditions between experiments and simulations would be almost impossible.

A more thorough model validation may be possible with the help of PINNs allowing leveraging all the information in the spatial-temporal dynamics of measured data. Basic idea of turbulence model validation using PINNs can be described as follows: (1) Consider a fluid turbulence model whose variables can be measured by a diagnostic in experiments. (2) Obtain a numerical solution of the model with experimental profiles and construct a reference (measurable) data set in the coordinates of the diagnostic, e.g., in $(R, z, t)$. (3) Find proper hyperparameters of PINN for it to learn the solution that matches the reference data. (4) Obtain the experimental measurements using the diagnostic and construct an experimental data set. Then, our hypothesis is that if the experimental data set is a subset of model solutions, PINN with the same hyperparameters should be able to learn a solution that matches the experimental data with the comparable accuracy. As a simple illustration, Fig. 5 shows that PINNs with wrong adiabatic coefficient $c_1$ in the HW model [2] cannot find a solution that matches the given data well, since PINNs are trained by minimizing both physics loss (the deviation from the given model equations) and data loss (the deviation from the given data).

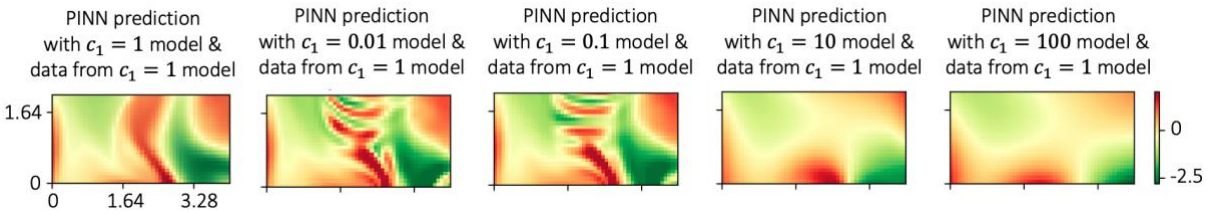


*FIG. 5. Simple illustration of PINN prediction of the density field in the HW model with different adiabatic coefficients*

## 6. SUMMARY

Methods for leveraging fluctuation measurements in fusion experiments are introduced with an application revealing the distinguished turbulence characteristics in the pedestal region in the spontaneous ELM-free and RMP ELM suppression phases. The spectral methods are useful to identify different modes and investigate a dominant nonlinear coupling among them. The statistical methods tell whether the measured turbulent fluctuations should be described as a stochastic system or a low-dimensional chaotic system. On the other hand, recent developments of the physics informed neural network allow leveraging two-dimensional fluctuation measurements in novel ways, predicting a missing field or validating turbulence models. Given a validated physics model and turbulence data, the PINN can accurately reconstruct fluctuations of a missing field such as plasma velocity, provided that the data have a sufficient signal-to-noise ratio and spatial resolution. These methods would contribute to a better understanding of plasma turbulence transport in fusion experiments.

## ACKNOWLEDGEMENTS

The author (M.J.C.) is grateful to Prof. H.K. Park, Prof. G.S. Yun, Dr. W. Lee, Dr. S. Zoletnik, and Prof. Y.-c Ghim, from whom he learned the fundamentals of plasma diagnostics and data analysis. DeepXDE (https://deepxde.readthedocs.io/) Python open-source framework is used for training PINNs in this work. Computing resources for the neural network training were provided on the KFE computer, KAIROS-GPU, funded by the Ministry of Science and ICT of the Republic of Korea (EN2541). The author (M.J.C.) appreciates the supports from Mr. J. Park and Dr. G. Jo in using the KAIROS-GPU. This work was supported by R&D Programs of "KSTAR Experimental Collaboration and Fusion Plasma Research (EN2501)" and "High Performance Fusion Simulation R&D (EN2541)" through Korea Institute of Fusion Energy (KFE) funded by the Government funds.

## REFERENCES

[1] KÖHN-SEEMANN, A., MORALES, R.B., From electron cyclotron emission and reflectometry to microwave imaging diagnostics in fusion plasmas: Progress and perspectives, Phys. Plasmas **32** (2025) 060502.
[2] CHOI, M.J., Leveraging turbulence data from fusion experiments, Rev. Mod. Plasma Phys. **9** (2025) 22.
[3] BENDAT, J.S., PIERSOL, A.G., Random Data: Analysis and Measurement Procedures (2nd Edition), John Wiley & Sons, Inc. (1986).
[4] FARGE, M., Wavelet transforms and their applications to turbulence, Annu. Rev. Fluid Mech. **24** (1992) 395.
[5] HAYKIN S., et al., Nonlinear Methods of Spectral Analysis (2nd Edition), Springer Berlin, (1983).
[6] VANDERPLAS, J.T., Understanding the Lomb–Scargle periodogram, ApJ Suppl. Ser. **236** (2018) 16.
[7] WATTS, C., A review of ece correlation radiometry techniques for detection of core electron temperature fluctuations, Fusion Sci. Tech. **52** (2007) 176.
[8] LI, T.H., "Robust coherence analysis in the frequency domain", the 18th European Signal Processing Conference (2010).
[9] FARGE, M., SCHNEIDER, K., DEVYNCK, P., Extraction of coherent bursts from turbulent edge plasma in magnetic fusion devices using orthogonal wavelets, Phys. Plasmas **13** (2006) 042304.
[10] KIM, Y.C., POWERS, E.J., Digital bispectral analysis and its applications to nonlinear wave interactions, IEEE Trans. Plasma Science **PS-7** (1979) 120.
[11] CHANDRAN, V., ELGAR, S., VANHOFF, B., Statistics of tricoherence, IEEE Trans. Signal Process **42** (1994) 3430.
[12] KOVACH, C.K., A slice of trispectrum for patterns of modulation, TechRxiv doi:10.36227/techrxiv.21401703 (2022).
[13] ROSSO, O.A., Distinguishing noise from chaos, Phys. Rev. Lett. **99** (2007) 154102.
[14] LÓPEZ-RUIZ, R., MANCINI, H.L., CALBET, X., A statistical measure of complexity, Phys. Lett. A **209** (1995) 321.

[15] BANDT, C., POMPE, B., Permutation entropy: a natural complexity measure for time series, Phys. Rev. Lett. **88** (2002) 174102.
[16] ZHU, Z., et al., Chaotic edge density fluctuations in the Alcator C-Mod tokamak, Phys. Plasmas **24** (2017) 042301.
[17] CHOI, M.J., et al., Stochastic fluctuation and transport of tokamak edge plasmas with the resonant magnetic perturbation field, Phys. Plasmas **29** (2022) 122504.
[18] DIAMOND, P.H., et al., Zonal flows in plasma—a review, Plasma Phys. Control. Fusion **47** (2005) R35.
[19] CHEN, L., LIN, Z., WHITE, R., Excitation of zonal flow by drift waves in toroidal plasmas, Phys. Plasmas **7** (2000) 3129.
[20] PARK, J.K., et al., 3D field phase-space control in tokamak plasmas, Nat. Physics **14** (2018) 1223.
[21] HU, Q.M., et al., The role of edge resonant magnetic perturbations in edge-localized-mode suppression and density pump-out in low-collisionality DIII-D plasmas, Nucl. Fusion **60** (2020) 076001.
[22] WAELBROECK, F.L., CONNOR, J.W., WILSON, H.R., Finite Larmor-radius theory of magnetic island evolution, Phys. Rev. Lett. **87** (2001) 215003.
[23] CAO, M., DIAMOND, P.H., Quasi-mode evolution in a stochastic magnetic field, Nucl. Fusion **64** (2024) 036003.
[24] ENTERS, Y.W., et al., Testing image-velocimetry methods for turbulence diagnostics, Rev. Sci. Instrum. **94** (2023) 075101.
[25] RAISSI, M., YAZDANI, A., KARNIADAKIS, G.E., Hidden fluid mechanics: Leanring velocity and pressure fields from flow visualizations, Science **367** (2020) 1026.
[26] SEO, J., Solving real-world optimization tasks using physics-informed neural computing, Sci. Reports **14** (2024) 202.
[27] JOUNG, S., et al., GS-DeepNet: mastering tokamak plasma equilibria with deep neural networks and the Grad–Shafranov equation, Sci. Rep. **13** (2023) 15799.
[28] MATHEWS, A., et al., Uncovering turbulent plasma dynamics via deep learning from partial observations, Phys. Rev. E **104** (2021) 025205.